Inhibition of Elastase induced Abdominal Aortic Aneurysm Progression through the CXCL12/CXCR4 Axis via MiR206 3p Sponge

Xuezhen Xuan
Second Hospital of Shanxi Medical University
Yaling Li
Second Hospital of Shanxi Medical University
Genmao Cao
Second Hospital of Shanxi Medical University
Jie Hu
Second Hospital of Shanxi Medical University
Sheng Yan
Second Hospital of Shanxi Medical University
Haijiang Jin
Second Hospital of Shanxi Medical University
Maolin Qiao
Second Hospital of Shanxi Medical University
Lin Zheng
Second Hospital of Shanxi Medical University
Ruijing Zhang
Second Hospital of Shanxi Medical University
Honglin Dong
honglindong@sxmu.edu.cn
Second Hospital of Shanxi Medical University

Research Article

Keywords:

Posted Date: March 22nd, 2024

DOI: https://doi.org/10.21203/rs.3.rs-4119276/v1

Additional Declarations: No competing interests reported.

Abstract

Background

Prior research has established a significant association between the progression of abdominal aortic aneurysms (AAA) and the apoptosis and phenotypic transformation of vascular smooth muscle cells (VSMCs). Notably, the CXCL12/CXCR4 signaling pathway's activation is markedly increased in a mouse model of AAA. Nonetheless, the precise contribution of this pathway to AAA development remains to be elucidated.

Materials and Methods

We utilized a single-cell sequencing dataset pertaining to AAA from the Gene Expression Omnibus database, employing the R package CellChat (v1.1.3) to analyze communication strength, signaling pathways, and modes of interaction among various VSMC phenotypes and immune cells. The activity level of the CXCL12/CXCR4 axis was evaluated in both human AAA patients and a mouse model. We examined the impact of CXCR4-specific inhibitors on AAA progression and the regulatory influence of MiR206-3p sponge on this axis.

Results

Single-cell RNA sequencing analysis revealed a significant upregulation of CXCL12/CXCR4 axis in AAA tissues. Further, Serum ELISA and in vivo experiments indicate a pronounced activation of the CXCL12/CXCR4 axis in both AAA patients and the elastase-induced AAA mouse model. CXCR4-specific inhibitors inhibited further expansion and rupture of the abdominal aorta and reduced the infiltration of macrophages in the aorta. Diminishing miR206-3p levels in VSMCs led to a decrease in CXCR4 expression within AAA tissues and a reduction in serum CXCL12 concentrations. Furthermore, transfecting VSMCs with miR206-3p sponge curtailed apoptosis and phenotypic transformation, markedly reducing AAA diameter and rupture frequency in mice. In vitro experiments corroborated that blocking the CXCL12/CXCR4 axis mitigated apoptosis and phenotypic transformation of VSMCs.

Conclusion

Our findings propose that MiR206-3p sponge represents an innovative therapeutic strategy to attenuate AAA progression and rupture risk, primarily through the suppression of the CXCL12/CXCR4 signaling pathway.

Introduction

An abdominal aortic aneurysm (AAA) constitutes an irreversible localized expansion of the abdominal aorta to ≥ 3 cm in diameter or > 1.5 times its expected normal diameter[1]. AAA, a form of aortic disease, is a significant cause of mortality in adults, with an overall mortality rate exceeding 80% following rupture, making it the 13th leading cause of death in the U.S. population[2, 3]. Typically, surgery or interventional therapy is the primary treatment for aneurysms with a larger diameter or rapid progression. However, there is a deficiency in medications that effectively prevent aortic degeneration or decelerate the progression of AAA, particularly in cases of smaller-diameter aneurysms or in patients with contraindications to surgery[4]. Despite recent advances in aortic disease research, the principal etiological factors of AAA remain obscure. Hence, it is imperative to conduct comprehensive studies on the underlying pathologic mechanisms.

The aortic wall is comprised of the intima, media, and adventitia, sequentially from the innermost layer, with an elastic lamina interspersed between each layer. Smooth muscle cells (SMCs), the most prevalent cell type in the aorta and primarily located in the media, are essential for maintaining arterial structural integrity through their contractile action and secretion of extracellular matrix components. The apoptosis and phenotypic transformation of SMCs are believed to significantly influence AAA progression[5, 6]. Evidence suggests that promoting SMC proliferation or inhibiting their apoptosis can lower the rupture rate of AAA[7, 8]. Yet, the proliferation and phenotypic transformation of SMCs may have a complex, bidirectional relationship with AAA progression, contingent on the type and quantity of SMCs involved. Contractile VSMCs, in particular, are capable of cooperating with elastic fibers to reinstate arterial diameter post-cardiac pumping due to their contractility, highlighting that a reduction in the number and density of contractile VSMCs indicates severe aortic pathology[9]. Historically, VSMCs were classified into contractile and synthetic types[10]. However, the advent of single-cell sequencing and lineage tracing technologies has facilitated the identification of a broader spectrum of SMC types[11, 12]. Lineage tracing techniques, which involve the administration of tamoxifen to "illuminate" SMCs in tissues, allow for the identification of SMCs through specific fluorescence, even after phenotypic transformation in response to inflammatory stimuli and other factors[13]. This technique is invaluable for exploring SMC phenotypic transformation, especially given the potential for the reduction or loss of SMC-specific markers (e.g., MYH11, ACTA2, TAGLN, and CNN1)[9]. Although phenotypically transformed SMCs exhibit reduced contractile function, they retain capabilities such as proliferation, migration, phagocytosis, and synthetic secretion[14, 15]. Recent studies indicate that VSMCs initially form clusters of intermediate cells expressing specific gene markers (e.g., KLF4 or LGALS3) before undergoing further transformation[16].

MicroRNAs (miRNAs) are endogenous regulatory RNAs, each comprising approximately 22 nucleotides. They regulate gene expression post-transcriptionally by binding directly to the 3’UTRs of target mRNAs[17]. It is estimated that miRNAs may regulate up to one-third of human genes[18]. Recent research indicates that miR206-3p plays a role in the progression of vascular diseases by influencing the proliferation and differentiation of skeletal and smooth muscle cells, though the underlying mechanisms remain to be elucidated[19]. Chemokines, small heparin-binding proteins, guide inflammatory cells to sites of lesions or injuries[20]. Approximately 50 human chemokines have been identified, categorized into four main families based on their structural and functional differences; one such family is the C-X-C

Motif Chemokine[21]. C-X-C Motif Chemokine Ligand 12 (CXCL12), also known as stromal cell-derived factor 1 (SDF-1), interacts with C-X-C Chemokine Receptor Type 4 (CXCR4) and C-X-C Chemokine Receptor Type 7 (CXCR7)[22]. CXCR4, also referred to as CD184, is a G-protein-coupled receptor found to be aberrantly expressed in various disorders[23]. The CXCL12/CXCR4 axis participates in numerous cellular functions, including cell proliferation, migration, and differentiation, and has been thoroughly investigated in several tumors and autoimmune diseases[24–26]. In a study involving 32 patients with AAA undergoing open surgery, CXCR4 and CXCL12 were found to be overexpressed in AAA tissue and associated with inflammation in the artery wall. Recent findings demonstrate that inhibiting the CXCL12/CXCR4 axis significantly reduces pulmonary vascular adventitial cell coverage and macrophage infiltration in pulmonary hypertension (PH) rats[27], suggesting that targeting this axis could offer a novel approach to treating aortic diseases.

Consequently, the impact of the CXCL12/CXCR4 axis on AAA development, specifically regarding diameter dilation and rupture rate, was investigated using an experimental AAA mouse model involving abdominal aortic elastase localized incubation plus oral BAPN treatment. The molecular mechanisms underlying these effects were further examined through in vivo and in vitro studies.

Methods

Human Serum Collection and Ethics Statement

All patients with abdominal aortic aneurysms are diagnosed by abdominal vascular ultrasound or CTA by experienced vascular surgeons and imaging physicians. This study was approved by the Ethics Committee of the Second Affiliated Hospital of Shanxi Medical University (approval document No. (2023) YX No. (271)) and conducted in accordance with the Declaration of Helsinki. All patients received written informed consent. Serum was collected from AAA patients who were expected to undergo endovascular isolation for abdominal aortic aneurysm. Control serum was collected from age-matched healthy individuals who had no aneurysm, dissection, coarctation, or previous aortic repair. The characteristics of all patients with abdominal aortic aneurysms who participated in this project and the matched healthy population were recorded in Table 1.

Animals and mouse model

Our research program was approved by the Animal Ethics Committee of the Second Hospital of Shanxi Medical University (approval number DW2023048). To construct pedigree tracer mouse strains, Myh11promoter-CreERT2 sequence was inserted into the Y chromosome of C57BL/6 mice, and obtained $Myh11^{CreERT2/+}$ mice after screening. Then $Myh11^{CreERT2/+}$ mice and $Rosa26^{LSL-tdtomato+/+}$ mice (purchased from Shanghai Nannan Model Biotechnology Co., LTD.) were hybridized to obtain male $Myh11^{CreERT2/+}$; $Rosa26^{tdTomato/+}$ mice. 6 weeks old male $Myh11^{CreERT2/+}$; $Rosa26^{tdTomato/+}$ mice were used for lineage tracing of vascular smooth muscle cells. Before the experiment, the mice were continuously intrabitoneally injected with Tamoxifen (50mg/kg/day) for 10 days to induce expression of

tdTomato protein. We stratified mice according to body weight and randomly divided them into sham group, AAA group, miR-NC group and miR206-3p sponge transfection group. Each mouse was anesthetized by inhalation of isoflurane and a midline incision was made through the abdominal skin and muscle. The abdominal aorta and surrounding tissue were carefully separated under a light microscope. Subsequently, gelatin sponge impregnated with elastase solution (50mg/ml) was placed close to the lower renal segment of abdominal aorta for 15min. The sham group used gelatin sponges impregnated with 0.9% saline. After the sponge was removed, the abdominal cavity was lavished three times with 0.9% saline. After resetting the abdominal organs, the muscles and skin were sutured with 6 – 0 nylon thread. The mice were fed 0.2% fumarate 3-amino-propionitrile (BAPN) for 30 days after surgery. AMD3100 (Abcam,ab120718), a specific inhibitor of CXCR4, was dissolved in PBS and injected intraperitoneally for 30 days(5mg/kg/day). Sham animals received vehicle treatment. The miR-NC group and miR206-3p sponge transfection group were injected with AAV2/9-ZsGreen NC (titer: 1.2×10^{12} vp/ml, 70 μl) and AAV2/9-CMV-mmu-miR-206-3P-SP onge ZsGreen (titer: 1.4×10^{12} vp/ml, 60 μl) to construct transfection model.

Cell culture, treatment and transfection

Mouse aortic smooth muscle cells (MOVAS) and mouse mononuclear macrophage leukemia cells (RAW264.7) were purchased from Jiangsu Kaiji Biotechnology Co., LTD. (article No. KG612) and Suzhou Haixing Biotechnology Co., LTD. (TCM-C766), respectively. We used DMEM medium containing 1% penicillin/streptomycin and 10% fetal bovine serum (FBS) for cell culture and placed the medium in a 37°C incubator containing 5% CO2. To construct a stable transfection cell line, we infected MOVAS with a miR206-3p sponge expressing lentivirus or lentiviral vector (MOI = 100) in complete culture medium for 72 hours. Transfection efficiency was calculated after 48 hours of culture. In addition, 2.0ug/ml puromycin (China, article No. HB-PU-500) was used to screen lentivirus stable strains. After obtaining the stable transmutation, the cells were amplified by passage. In order to provide AAA microenvironment, we added induced RAW264.7 (2.5ng/ml IFN-γ + 200ng/ml LPS) culture medium to MOVAS and continued to culture for 24 hours.

Animal ultrasound

The maximum abdominal aortic diameter was assessed using the Vevo 3100 platform (FUJIFILM VisualSonics) and the MX550D transducer (FUJIFILM VisualSonics) before mouse AAA modeling and before execution. Mice were anesthetized with isoflurane (3% isoflurane for induction and 2% isoflurane for maintenance) and placed on a heated plate at 37 ℃. We selected the most severely dilated area of the subrenal abdominal aorta and used longitudinal B-mode ultrasound to obtain maximum intra-aortic diameter during systole. In all abdominal ultrasound experiments, the mice were tested in a random order.

microRNA analysis by real-time PCR

The aorta tissues of mice were rapidly isolated, and total microRNA (Mei5 Biotechnology, Cat.MF044-01) was extracted by centrifugal-adsorbed silica matrix membrane separation after liquid nitrogen grinding. The HyperScriptTM III miRNA 1st Strand cDNA Synthesis Kit(by stem-loop)(NovaBio # R601) reverse

transcriptase was then used to reverse transcribe the cDNA. The expression of miR206-3p was detected by RT-PCR (NovaBio # Q206). The expression level of miRNA was normalized to U6 level and calculated by △△CT method. All reagents are used in accordance with the manufacturer's instructions. The amplification reaction procedure consists of predenaturation at 95℃, 30s, followed by 40 cycles at 95 ℃, 10s, and 60℃, 30s. The primers for miR206-3p (RT primer: (Stem-loop RT Primer: 5’GTCGTATCCAGTGCAGGGTCCGAGGTATTCGCACTGGATACGACCCACAC3’; qPCR forward primer:5’GCGCGTGGAATGTAAGGAAGT3’; qPCR reverse primer:5’AGTGCAGGGTCCGAGGTATT3’), U6 (RT primer: (Stem-loop RT Primer:5’GTCGTATCCAGTGCAGGGTCCGAGGTATTCGCACTGGATACGACA

AAATATGG3’; qPCR forward primer:5’GCTCGCTTCGGCAGCACATATAC3’; qPCR reverse primer:5’AGTGCAGGGTCCGAGGTATT3’)were designed by EnzyArtisan (Shanghai, China). The RNA isolation of MOVAS and real-time PCR were the same as before.

Western Blot

Protein was extracted from MOVAS and abdominal aorta tissues using RIPA lysis buffer (Thermo Scientific, Cat#89901). To put it simply, the rat abdominal aortic segment tissue or MOVAS was rapidly divided after the experiment was terminated, treated with ultrasonic crusher (manufacturer, model), cracked with RIPA cracking solution, and then obtained cell or histopin solution after centrifugation with supernatant and boiling water bath denaturation. An equal amount of protein extract (20 ~ 30μg/lane) was analyzed by Western blot analysis on 10%SDS-PAGE (Servicebio, Cat#G2003-50T, Wuhan, China) and transferred to PVDF membrane. After being blocked with 5% skim milk powder at room temperature for 2h, the primary antibody CXCR4(Abcam,ab181020), a-SMA (Abcam,ab124964) and KLF4(Abcam,ab214666) were incubated at 4℃ overnight, and the secondary antibody was incubated at room temperature for 1h. The image was obtained by the ChemiDoc XRS + system (Bio-Rad). In this study, the ECL protocol was used, GAPDH was used as endogenous reference, and goat anti-mouse or rabbit anti-mouse IgG was used to detect antigen antibody complex.

Cytotoxicity assay

Cell viability was measured by CCK-8 Cytotoxicity and viability assay kit (GLPBIO,GK10001). Simply put, MOVAS suspension was inoculated into a 96-well plate at a density of $4*10^3$ cells/well and cultured in 100ul medium for 24h (37℃, 5% CO2). After that, the activated macrophage supernatant and AMD3100 solution of different concentrations were added to the plate. After the 96-well plates were incubated in the incubator for 24h, they were washed 3 times with PBS, and the culture medium was replaced with fresh medium containing 10% CCK-8 proliferation kit. After two hours of incubation, the absorbance at 450 nm was measured using an enzymograph. Cell viability was measured and normalized with control group. Finally, Prime 9 was used for statistical analysis of cell viability under each AMD3100 concentration.

TUNEL assay

Cells or abdominal aorta segments were fixed with 4% paraformaldehyde and paraffin embedded, histological sections (3um) were performed. After the sections were dewaxed, 20μg/ml protease K was

added and incubated in 37℃ incubator for 30min. After that, the TUNEL test solution was added to 37°C incubator and incubated for 60min in the dark, and then washed with PBS for 3 times. Droplet nuclei were backstained with DAPI. After dehydration and transparency, anti-fluorescence quenching sealing tablets are added. Red fluorescence was observed using confocal microscopy. Images were obtained by Leica Application Suite X Software (Leica, DMIL LED Inverted Microscope).

ELISA

After the experiment, the mice were euthanized and their blood was centrifuged to obtain serum. Human stromal cell derived derived factor 1 (SDF-1) ELISA kit (MEIMIAN,Cat#MM-2124H1,Jiangsu,China) was used in strict accordance with the instructions to detect the serum CXCL12 levels of the patients. CXCL12 levels in mouse serum and cell supernatant were detected using mouse stromal cell derived derived Factor 1 (SDF-1) ELISA kit (MEIMIAN,Cat#MM-44155M1,Jiangsu,China).

Immunofluorescence Staining

After euthanized mice, abdominal aorta tissue was removed and OCT embedding was performed. The tissues were then frozen and fixed with 4% paraformaldehyde for 30min. The sections were repaired with EDTA antigen repair buffer (PH6.0) and blocked with 5% BSA for 30min. The slices were then incubated overnight with anti-CXCR4 (Abcam, ab181020), anti-αSMA (Abcam, ab124964 and ab7817), anti-KLF4 (Abcam, ab214666) and anti-CD68 (Abcam, ab283654) antibodies at 4°C. Secondary antibodies (Abcam, ab150117 and ab150080) were incubated in the dark at room temperature for 50min. The nucleus is marked blue by DAPI. The immunofluorescence effect was observed immediately after sealing. When cell immunofluorescence staining was performed, MOVAS cells located on the cell crawl were first immobilized with 4% paraformaldehyde, followed by penetration with 0.3% Triton X-100 for 3min and blocked with 1:20 diluted goat serum. Anti-CXCR4 (Abcam, ab181020) and anti-αSMA (Abcam, ab124964 and ab7817) antibodies were incubated overnight at 4℃. Secondary antibodies (Abcam, ab150117 and ab150080) were incubated in the dark at room temperature for 2h. Nuclear staining with DAPI. The immunofluorescence effect was observed immediately after sealing. Immunofluorescence images were obtained by Leica Application Suite X software (Leica, DMIL LED inverted microscope).

Hematoxylin & Eosin Staining and Elastic Fiber Staining

After the end of the experiment, the abdominal aortic segment of the rats was quickly removed, and the maximum diameter segment of the abdominal aortic aneurysm was cut off, fixed in 4% paraformaldehyde and paraffin embedded for histological section (3um). hematoxylin & eosin staining (HE), elastic-Van Gieson (EVG) staining was conducted in strict accordance with the requirements of reagent suppliers.

Statistical Analysis

The results were expressed as mean ± SD, and statistical analysis was performed using GraphPad Prism 9.0. Results are expressed as mean ± standard deviation. The Student t test was used for statistical

comparison between the two groups. One-way analysis of variance was performed for three or more groups. $P \leq 0.05$ was considered statistically significant.

Results

1.Detection of CXCR12/CXCL4 expression in Vascular Smooth Muscle Cells of Aortic Aneurysms

We obtained single-cell datasets for five mouse AAA samples from the GEO database, comprising three AAA samples and two samples from normal arteries. Utilizing the Seurat package in R, we categorized single cells into clusters and conducted mapping Prior to single-cell data analysis, we applied filters to remove dead or stressed cells based on several criteria: (1) the presence of more than 500 but fewer than 30,000 genes detected per cell; (2) a total of more than 1,000 UMI detected per cell; and (3) mitochondrial gene expression below 5% per cell. Following this filtration, our dataset included 3,685 cells and 20,286 genes. Subsequently, these cells were organized into 15 distinct cell populations using UMAP analysis (Fig. 1A). We compared marker genes identified from previous studies with the top 50 marker genes in our dataset, ultimately identifying six cell types, including adipocytes (Adipoq, Apoc1), endothelial cells (Pecam1, Vwf), fibroblasts (Col1a1, Col1a2), macrophages (Cd86, Cd14, Tlr2), T/B cells (Cd19, Pdgfrn, Cd3e, Cd8a), and VSMCs (Acta2, Myh11) (Fig. 1B, C). Our analysis revealed significantly higher expression of the CXCR4 and CXCL12 genes in AAA mice compared to normal mice, indicating enhanced activity of this inflammatory pathway (Fig. 1D, E).

Additionally, we visualized cell communication among different cells (Fig. 1F) and observed CXCL signaling pathways between smooth muscle cells and other cells (Fig. 1G). A hierarchy plot demonstrated that VSMCs were the primary initiators of the CXCL signaling pathway (Fig. 1H).

To bridge the gap between bioinformatics findings and clinical reality, we also measured serum CXCL12 levels in patients undergoing endoluminal repair of abdominal aortic aneurysms or abdominal aortic replacement. ELISA results indicated that serum CXCL12 levels in AAA patients (n = 19) were significantly higher than those in healthy controls (Fig. 1J), aligning with our expectations. These findings suggest the CXCL12/CXCR4 axis may play a significant role in the development of AAA.

2. Elastase-induced increase of CXCL12/CXCR4 axis levels in AAA mice

The elastase-induced AAA mice model, a widely utilized framework for investigating abdominal aortic aneurysms, effectively generates authentic aneurysms within the abdominal aorta, contrasting with aneurysms induced by Ang II that are intercalated[28]. In these models, aneurysm diameters expand over time but rarely rupture in the short term, highlighting the importance of evaluating rupture rates due to its criticality as the most severe complication of AAA. Lysyl oxidase (LOX), which facilitates the cross-linking of collagen and elastin, can be inhibited by β-aminopropionitrile (BAPN), an oral LOX inhibitor. When

combined with elastase, BAPN increases the rupture rates of AAA in mice, making it an ideal candidate for examining the effects of interventions on AAA rupture[29]. Utilizing an elastase/BAPN-induced model, this study aimed to elucidate the impact of the CXCL12/CXCR4 axis on AAA progression (Fig. 2A). Examination of the gross specimens revealed significant dilatation of the abdominal aorta in the model group, with aneurysms predominantly located in the infrarenal region (Fig. 2B). The infrarenal abdominal aorta in certain mice experienced rapid dilation and subsequent rupture in a brief timeframe. Within 30 days of oral BAPN administration, 60% (n = 12) of AAA mice, compared to 0% (n = 0) in the sham operation group, succumbed to ruptured abdominal aortic aneurysms (Fig. 2C), underscoring the effectiveness of the elastase/BAPN model in investigating AAA rupture rates. Abdominal ultrasound assessments to measure the maximum diameter of infrarenal abdominal aortic aneurysms before euthanasia showed that the maximum diameter in the AAA group was approximately five times greater than that of the sham operation group (Fig. 2D, E). Hematoxylin and eosin, along with elastic-Van Gieson (EVG) staining, illustrated notable aortic diameter enlargement, increased disruption of the medial elastic membrane, and structural disarray of elastic fibers in AAA mice compared to the sham operation group (Fig. 2F). To evaluate changes in the CXCL12/CXCR4 axis in AAA mice, CXCL12 levels were quantified in mouse serum via ELISA, revealing a significant elevation in AAA mice (Fig. 2G), aligning with findings in AAA patients. Similarly, Western blot analysis indicated increased CXCR4 protein levels in AAA tissues (Fig. 2H, I). This study utilized male $Myh11^{CreERT2/+}$ and $Rosa26^{tdTomato/+}$ mice for the first time to conduct lineage tracing of vascular smooth muscle cells, with tamoxifen injection at 6 weeks leading to permanent tdTomato fluorescence in smooth muscle cells and their descendants. Immunofluorescence for CXCR4 was employed to determine its enhanced expression in smooth muscle cells (Fig. 2J, 2K). These findings suggest a significant role of the CXCL12/CXCR4 axis in the development of AAA, evidenced by its pronounced upregulation in both human and murine AAA tissues.

3. Enhancement of the CXCL12/CXCR4 axis is accompanied by increased phenotypic transformation and apoptosis of smooth muscle cells

Contractile VSMCs undergo a phenotypic transformation in response to external injury and stimulation by circulating inflammatory factors, a process considered crucial for the progression of AAA. During this transformation, αSMA, a marker of contractile smooth muscle cells, sees a reduction in expression, whereas KLF4, indicative of a regulatory VSMC phenotype, exhibits an increase[30]. This suggests that VSMCs enter a transitional state of transformation. Utilizing lineage tracing and immunofluorescence technologies enables more precise identification of transformed smooth muscle cells[13]. Western Blot analysis of abdominal aortic tissues revealed that VSMCs in AAA tissues displayed lower α-SMA and higher KLF4 expression compared to normal tissues (Fig. 3A-C). Lineage tracing highlighted a reduction or disappearance of αSMA expression, characteristic of over 85% of contractile VSMCs, during AAA formation (Fig. 3D, G), suggesting potential misidentification of non-αSMA expressing smooth muscle cells in the past. Furthermore, increased KLF4 expression in VSMCs (Fig. 3E, H) indicates a transformation of some contractile VSMCs into other phenotypes. Concurrently, TUNEL staining confirmed heightened apoptosis in aortic smooth muscle cells (Fig. 3F, I). In summary, the progression of

AAA is marked by a reduction in the number or density of contractile smooth muscle cells in the aortic wall, driven by apoptosis and phenotypic transformation under the influence of the enhanced CXCL12/CXCR4 axis.

4. Inhibition of abdominal aortic aneurysm progression in mice by AMD 3100

The CXCR4 antagonist Plerixafor (AMD 3100) was utilized to elucidate the role of the CXCL12/CXCR4 axis in abdominal aortic aneurysm progression. AMD3100, a specific small-molecule inhibitor of the CXCL12/CXCR4 signaling pathway[31], was administered intraperitoneally at a dose of 1.25 mg/kg/day for 30 consecutive days. This treatment effectively reduced the maximum diameter of infrarenal abdominal aortic aneurysms in mice (Fig. 4A), resulting in a significantly lower aneurysm rupture rate in the AMD3100-treated group (n = 20) compared to the control group receiving intraperitoneal injections of PBS (n = 20) (Fig. 4B, C). Notably, the rupture rate was higher in the PBS group (65%) compared to the model group (60%), potentially due to variations in blood pressure or body positioning during injection. Ultrasound examinations prior to euthanasia revealed that AMD3100 treatment decreased the maximum internal diameter of abdominal aortic aneurysms by approximately 70% (Fig. 4D, E). Histological analysis using hematoxylin and eosin (HE) and elastic-Van Gieson (EVG) staining showed that aneurysms in the PBS group had larger diameters, more disorganized elastic fibers, and increased intraluminal thrombus formation (Fig. 4F). Additionally, the study observed that the inhibitor reduced CD68 + cell infiltration in the aortic wall, primarily in the adventitia and media (Fig. 4G). These findings indicate that targeting the CXCL12/CXCR4 axis mayoffer an effective strategy for mitigating the progression of abdominal aortic aneurysms.

5. Inhibition of abdominal aortic aneurysm progression in mice by miR206-3p-sponge transfection

MiRNA exert a crucial regulatory function in cells by destabilizing mRNA and influencing mRNA translation[32]. Notably, a single miRNA can regulate multiple mRNAs simultaneously, and conversely, multiple miRNAs can target a single mRNA, with these interactions varying significantly across different diseases[33]. Previous research has identified a significant increase in miR206-3p levels in abdominal aortic aneurysm tissues. To investigate miR206-3p's role in the development of abdominal aortic aneurysms, miR206-3p levels were reduced in these tissues using a miR206-3p sponge gene vector delivered via adeno-associated virus type 2/9 (AAV-2/9), which shows high affinity for cardiomyocytes and vascular smooth muscle cells. The miR206-3p sponge, resembling a sponge-like structure with miR206-3p binding sites, effectively diminishes miR206-3p's cellular activity through specific binding. A comparison of abdominal aorta samples from the two mouse groups revealed a reduced aortic diameter in the miR206-3p sponge transfected mice (Fig. 5A). Survival analysis indicated a 35% decrease in the AAA rupture rate in the transfected group (n = 20) compared to the control group (n = 20) (Fig. 5B, C). Ultrasound examinations demonstrated that the maximum internal diameter of the abdominal aorta in the transfected group was approximately 67% of that in the control group (Fig. 5E). Hematoxylin and

eosin (HE) and elastic-Van Gieson (EVG) staining illustrated a notably smaller diameter, less disrupted elastic membrane, and more orderly elastic fiber structures in the transfected mice (Fig. 5F). Collectively, these findings suggest that reducing miR206-3p levels in abdominal aortic aneurysm tissues may effectively mitigate the progression of the condition in mice.

6. Reduction of CXCR4 expression in abdominal aortic aneurysms and phenotypic transformation and apoptosis in VSMCs by miR206-3p sponge

The study discovered that abdominal aortic aneurysms exhibiting low miR206-3p expression demonstrated reduced diameters and decreased rupture rates, prompting further investigation into the molecular mechanisms involved. Quantitative polymerase chain reaction (qPCR) analysis revealed that miR206-3p sponge transfection diminished miR206-3p levels in abdominal aortic aneurysm tissues by approximately 60% (Fig. 6A). Subsequent analyses, including Western blot (Fig. 6B, D, E) and immunofluorescence staining (Fig. 6H), indicated increased KLF4 and decreased αSMA expression in the tissues of the transfected group. This suggests a preservation of contractile VSMC phenotype with reduced phenotypic transformations following miR206-3p knockdown. Furthermore, qPCR and Western blot analyses showed that miR206-3p sponge transfection also lowered CXCR4 expression in abdominal aortic aneurysm tissues (Fig. 6B, C, H). ELISA results confirmed reduced serum CXCL12 levels in the transfected mice (Fig. 6G). Additionally, TUNEL staining indicated a decrease in apoptosis within the aortic tissues of the transfected group compared to the control group. These findings suggest that lowering miR206-3p levels in the aorta effectively inhibits phenotypic transformation and apoptosis of contractile VSMCs, potentially through the suppression of the CXCL12/CXCR4 axis in abdominal aortic aneurysms.

7. Reduction of phenotypic transformation and apoptosis in MOVAS by miR206-3p-sponge

The influence of CXCL12 on VSMC differentiation was further investigated through in vitro experiments. Drawing on prior research, RAW264.7 cells were stimulated with IFN-γ/LPS for 12 hours to induce CXCL12 production and secretion, as macrophages can generate and release CXCL12 under stress conditions, with activated RAW264.7 cells exhibiting increased iNOS expression. Following this, the culture medium was replaced, and the activated RAW264.7 cells were cultured for an additional 24 hours. The collected culture medium was then used for the subsequent co-culture of MOVAS cells (Fig. 7A). ELISA analysis revealed significantly higher CXCL12 levels in the co-culture medium compared to the control (PBS) group (Fig. 7B). Immunofluorescence staining of the cells showed a marked increase in CXCR4 expression and a decrease in αSMA expression, a marker specific to contractile smooth muscle cells, after 24 hours of co-culture, aligning with our expectations (Fig. 7C-F). CCK-8 assays indicated a reduction in MOVAS viability post co-culture, which was partially reversed by AMD3100 treatment (Fig. 7G). To assess the impact of reduced miR206-3p levels on smooth muscle cells within the abdominal aortic aneurysm microenvironment, miR206-3p sponge was introduced via lentiviral transfection. Western blot analysis demonstrated elevated αSMA protein levels and decreased CXCR4

protein levels in MOVAS cells from the transfected group compared to the control group (Fig. 7H-J). Furthermore, co-culture heightened smooth muscle cell apoptosis, with a significantly reduced apoptosis rate observed in the transfected MOVAS group (Fig. 7K), alongside enhanced cell viability (Fig. 7L). These findings indicate that the in vitro results corroborate the in vivo observations.

Disscusion

The extracellular matrix (ECM) structure of the aorta undergoes significant disruption during the progression of abdominal aortic aneurysms (AAA), characterized by the rupture of the elastic membrane and excessive degradation of elastin[34]. This leads to collagen compensatory proliferation and a subsequent decrease in aortic wall elasticity. Moreover, contractile smooth muscle cells experience apoptosis and phenotypic transformation in response to various stimuli, resulting in a reduced number or density. Such alterations culminate in diminished arterial wall stiffness, ultimately causing irreversible dilatation under blood pressure[35]. Our study validates that inhibiting the CXCL12/CXCR4 axis can mitigate AAA progression and lower rupture risk, as evidenced by both in vivo and in vitro experiments, highlighting the therapeutic potential of CXCR4 targeting for AAA management. Additionally, we demonstrate that miR206-3p deficiency plays a pivotal role in hindering AAA progression, potentially through CXCL12/CXCR4 axis inhibition, underscoring the therapeutic promise of miR206-3p sponge in AAA treatment.

Chemokines, structurally akin small molecule secreted proteins with molecular weights around 8–10 kDa, facilitate cell migration and activation by binding to their complementary G protein-coupled cell surface receptors. These molecules are crucial for therapeutic interventions in human diseases, as they modulate inflammatory responses in pathological conditions[36]. CXCL12's interaction with CXCR4 initiates downstream signaling pathways involved in various cellular processes, including proliferation, migration, and differentiation[37]. Originally identified as a co-receptor for HIV-1 in CD4 + T cell infection[38], CXCR4 expression has been detected in numerous cancer cells[39], often overexpressed at tumor sites alongside elevated stromal tissue CXCL12 levels. Recent research by Bordenave et al. and Michineau et al. has shown that blocking the CXCL12/CXCR4 axis significantly reduces pulmonary vascular epicardial cell coverage and macrophage infiltration in pulmonary hypertension (PH) rats[27], Michineau et al. demonstrated through a GFP+/- bone marrow transplantation experiment that overexpression of CXCL12 in abdominal aortic aneurysms was linked to the recruitment of bone marrow-derived macrophages. Furthermore, real-time quantitative polymerase chain reaction analysis indicated elevated levels of both CXCL12 and CXCR4 mRNA in the AAA wall of human and CaCl2-induced mice[40]. Given the critical role of CXCR4 in the signaling network associated with arterial disease, we are keenly interested in developing therapeutic strategies for this target.

AMD3100 was initially identified as a contaminant in a commercial cyclam sample[41], which was subsequently discovered to specifically inhibit CXCR4 signaling[42], as demonstrated by calcium flux assays. As a result, AMD3100 has become increasingly utilized in basic research targeting the CXCL12/CXCR4 pathway disorders, including as a specific inhibitor of CXCR4. Chronic autoimmune

diseases such as rheumatoid arthritis (RA) and systemic lupus erythematosus (SLE) involve multiple sites with high levels of inflammatory cells and cytokines. AMD3100 or its derivatives have been shown to inhibit the migration of CXCR4 + cells into the synovial fluid of RA patients, reduce neovascularization, and lessen the severity of lupus nephritis in an arthritic mouse model[39]. Bordenave et al. similarly found that AMD3100 significantly reduced macrophage infiltration in the pulmonary arteries[27]. Our research confirms that AMD3100 curtails the progression of abdominal aortic aneurysms and lowers their rupture risk while diminishing CD68 + cell infiltration in the aortic wall, aligning with earlier findings. Traditionally, smooth muscle cells were categorized as either contractile or synthetic. However, with advances in single-cell sequencing and lineage tracing technologies, an increasing variety of smooth muscle cell types has been identified, including Macrophage-like, Mesenchymal-like, Fibroblast-like, Adipocyte-like, T-cell-like, and osteochondrogenic cell-like VSMCs[43]. The phenotypic transformation of vascular smooth muscle cells is characterized by a decline in the expression of contractile-specific markers (e.g., MYH11, αSMA) and an increase in markers associated with other cell types (e.g. CD68, CD34, FABP4, CD3D). These cells exhibit reduced contractile function and acquire capabilities such as phagocytosis and synthetic secretion. Recent studies have elucidated that VSMCs initially form clusters of intermediate cells (ie, modulated VSMCs) expressing genetic markers (e.g., KLF4 and Lgals3), which then transform into other types. This process was corroborated in our study, where KLF4 protein levels were markedly elevated in abdominal aortic aneurysm tissues, but contractile phenotypic marker αSMA levels were decreased. Thus, the phenotypic transformation of VSMCs is integral to the development of abdominal aortic aneurysms. The transfection of MiR206-3p-sponge is shown to provide a protective effect by inhibiting the phenotypic transformation of VSMCs in these aneurysms.

Located on chromosome 6p12.2, the gene encoding miR206 exhibits a highly conserved genomic sequence as a vertebrate-specific microRNA[44]. MiR206-3p has been extensively demonstrated in previous studies to inhibit the proliferation of various cancers[17, 45]. Additionally, research by HK Kim et al. determined that overexpression of miR206 enhances the differentiation of C2C12 myoblasts (MB). Subsequent findings indicated that decreasing miR206 levels encourages smooth muscle cell proliferation. Our findings further reveal that reducing intracellular miR206-3p levels through the transfection of MiR206-3p-sponge improves VSMC viability and lowers apoptosis rates in VSMCs in both in vivo and in vitro settings, contributing to the preservation of arterial wall elasticity and mitigating the risk of expansion and rupture of abdominal aortic aneurysms.

Our research also validated the significance of the CXCL12/CXCR4 axis in AAA progression, demonstrating that blocking CXCR4 with the specific inhibitor AMD3100 reduces the likelihood of AAA expansion and rupture. This underscores the protective role of MiR206-3p-sponge in AAA and initiates an exploration into the potential mechanisms involved. However, an in-depth analysis of the underlying molecular mechanisms was not conducted. Despite the emerging use of microRNAs in gene therapy for certain genetic disorders, there remains a considerable journey ahead. Our study contributes to understanding the pathogenesis of abdominal aortic aneurysms and suggests new therapeutic strategies for the condition. In summary, we posit that targeting the CXCL12/CXCR4 pathway in VSMCs through the

transfection of MiR206-3p sponge or the use of small molecule inhibitors holds promise as a therapeutic approach for preventing and treating AAA.

Declarations

Author Contribution

Xuezhen Xuan, Yaling Li, and Genmao Cao(Co-first author): Conceptualization, Validation, Investigation, Formal Analysis, Writing - Original Draft; Jie Hu, Sheng Yan, Haijiang Jin: Data Curation, Visualization, Resources; Maolin Qiao, Lin Zheng: Visualization, Formal Analysis; Ruijing Zhang, Honglin Dong: Review & Editing, Funding Acquisition, Project Administration. All authors reviewed the manuscript.

References

1. Dikilitas, O., B.A. Satterfield, and I.J. Kullo, *Risk Factors for Polyvascular Involvement in Patients With Peripheral Artery Disease: A Mendelian Randomization Study.* J Am Heart Assoc, 2020. **9**(24): p. e017740.
2. Rao, J., et al., *Distinct macrophage phenotype and collagen organization within the intraluminal thrombus of abdominal aortic aneurysm.* J Vasc Surg, 2015. **62**(3): p. 585-93.
3. Raaz, U., et al., *Segmental aortic stiffening contributes to experimental abdominal aortic aneurysm development.* Circulation, 2015. **131**(20): p. 1783-95.
4. Isselbacher, E.M., et al., *2022 ACC/AHA Guideline for the Diagnosis and Management of Aortic Disease: A Report of the American Heart Association/American College of Cardiology Joint Committee on Clinical Practice Guidelines.* J Am Coll Cardiol, 2022. **80**(24): p. e223-e393.
5. Li, D.Y., et al., *H19 Induces Abdominal Aortic Aneurysm Development and Progression.* Circulation, 2018. **138**(15): p. 1551-1568.
6. Zhang, W., et al., *INKILN is a Novel Long Noncoding RNA Promoting Vascular Smooth Muscle Inflammation via Scaffolding MKL1 and USP10.* Circulation, 2023. **148**(1): p. 47-67.
7. Li, K., et al., *LncRNA CRNDE affects the proliferation and apoptosis of vascular smooth muscle cells in abdominal aortic aneurysms by regulating the expression of Smad3 by Bcl-3.* Cell Cycle, 2020. **19**(9): p. 1036-1047.
8. Liu, S., et al., *Spermidine Suppresses Development of Experimental Abdominal Aortic Aneurysms.* J Am Heart Assoc, 2020. **9**(8): p. e014757.
9. Lei, C., et al., *FAM3A reshapes VSMC fate specification in abdominal aortic aneurysm by regulating KLF4 ubiquitination.* Nat Commun, 2023. **14**(1): p. 5360.
10. Tsai, M.C., et al., *Shear stress induces synthetic-to-contractile phenotypic modulation in smooth muscle cells via peroxisome proliferator-activated receptor alpha/delta activations by prostacyclin released by sheared endothelial cells.* Circ Res, 2009. **105**(5): p. 471-80.

11. Shankman, L.S., et al., *KLF4-dependent phenotypic modulation of smooth muscle cells has a key role in atherosclerotic plaque pathogenesis.* Nat Med, 2015. **21**(6): p. 628-37.
12. Yu, L., et al., *An intersegmental single-cell profile reveals aortic heterogeneity and identifies a novel Malat1(+) vascular smooth muscle subtype involved in abdominal aortic aneurysm formation.* Signal Transduct Target Ther, 2022. **7**(1): p. 125.
13. Chakraborty, A., et al., *Epigenetic Induction of Smooth Muscle Cell Phenotypic Alterations in Aortic Aneurysms and Dissections.* Circulation, 2023. **148**(12): p. 959-977.
14. Liu, M. and D. Gomez, *Smooth Muscle Cell Phenotypic Diversity.* Arterioscler Thromb Vasc Biol, 2019. **39**(9): p. 1715-1723.
15. Hartmann, F., et al., *SMC-Derived Hyaluronan Modulates Vascular SMC Phenotype in Murine Atherosclerosis.* Circ Res, 2021. **129**(11): p. 992-1005.
16. Woo, S.H., et al., *TXNIP Suppresses the Osteochondrogenic Switch of Vascular Smooth Muscle Cells in Atherosclerosis.* Circ Res, 2023. **132**(1): p. 52-71.
17. Bahari Khasraghi, L., et al., *MicroRNA-206 in human cancer: Mechanistic and clinical perspectives.* Cell Signal, 2023. **101**: p. 110525.
18. Calin, G.A. and C.M. Croce, *MicroRNA signatures in human cancers.* Nat Rev Cancer, 2006. **6**(11): p. 857-66.
19. Sun, H., et al., *MicroRNA-206 regulates vascular smooth muscle cell phenotypic switch and vascular neointimal formation.* Cell Biol Int, 2017. **41**(7): p. 739-748.
20. Charo, I.F. and R.M. Ransohoff, *The many roles of chemokines and chemokine receptors in inflammation.* N Engl J Med, 2006. **354**(6): p. 610-21.
21. Meyrath, M., et al., *The atypical chemokine receptor ACKR3/CXCR7 is a broad-spectrum scavenger for opioid peptides.* Nat Commun, 2020. **11**(1): p. 3033.
22. Cambier, S., M. Gouwy, and P. Proost, *The chemokines CXCL8 and CXCL12: molecular and functional properties, role in disease and efforts towards pharmacological intervention.* Cell Mol Immunol, 2023. **20**(3): p. 217-251.
23. Correia, A.L., et al., *Hepatic stellate cells suppress NK cell-sustained breast cancer dormancy.* Nature, 2021. **594**(7864): p. 566-571.
24. Nengroo, M.A., et al., *Demystifying the CXCR4 conundrum in cancer biology: Beyond the surface signaling paradigm.* Biochim Biophys Acta Rev Cancer, 2022. **1877**(5): p. 188790.
25. Kim, M.Y., *CXCR4 to improve both T cell homing and function.* Blood, 2023. **141**(21): p. 2546-2547.
26. Arazi, A., et al., *The immune cell landscape in kidneys of patients with lupus nephritis.* Nat Immunol, 2019. **20**(7): p. 902-914.
27. Bordenave, J., et al., *Neutralization of CXCL12 attenuates established pulmonary hypertension in rats.* Cardiovasc Res, 2020. **116**(3): p. 686-697.
28. Lu, G., et al., *A novel chronic advanced stage abdominal aortic aneurysm murine model.* J Vasc Surg, 2017. **66**(1): p. 232-242.e4.

29. Golledge, J., S.M. Krishna, and Y. Wang, *Mouse models for abdominal aortic aneurysm.* Br J Pharmacol, 2022. **179**(5): p. 792-810.
30. Alencar, G.F., et al., *Stem Cell Pluripotency Genes Klf4 and Oct4 Regulate Complex SMC Phenotypic Changes Critical in Late-Stage Atherosclerotic Lesion Pathogenesis.* Circulation, 2020. **142**(21): p. 2045-2059.
31. Liang, G.Q., et al., *Anti-CXCR4 Single-Chain Variable Fragment Antibodies Have Anti-Tumor Activity.* Front Oncol, 2020. **10**: p. 571194.
32. Rupaimoole, R. and F.J. Slack, *MicroRNA therapeutics: towards a new era for the management of cancer and other diseases.* Nat Rev Drug Discov, 2017. **16**(3): p. 203-222.
33. Li, J., et al., *miR-29b contributes to multiple types of muscle atrophy.* Nat Commun, 2017. **8**: p. 15201.
34. Hellenthal, F.A., et al., *Biomarkers of AAA progression. Part 1: extracellular matrix degeneration.* Nat Rev Cardiol, 2009. **6**(7): p. 464-74.
35. Zhang, F., et al., *Ganglioside GM3 Protects Against Abdominal Aortic Aneurysm by Suppressing Ferroptosis.* Circulation, 2024. **149**(11): p. 843-859.
36. Weber, C., A.J.R. Habenicht, and P. von Hundelshausen, *Novel mechanisms and therapeutic targets in atherosclerosis: inflammation and beyond.* Eur Heart J, 2023. **44**(29): p. 2672-2681.
37. Levoye, A., et al., *CXCR7 heterodimerizes with CXCR4 and regulates CXCL12-mediated G protein signaling.* Blood, 2009. **113**(24): p. 6085-93.
38. Feng, Y., et al., *HIV-1 entry cofactor: functional cDNA cloning of a seven-transmembrane, G protein-coupled receptor.* Science, 1996. **272**(5263): p. 872-7.
39. Wang, J., et al., *CXCR4 antagonist AMD3100 (plerixafor): From an impurity to a therapeutic agent.* Pharmacol Res, 2020. **159**: p. 105010.
40. Michineau, S., et al., *Chemokine (C-X-C motif) receptor 4 blockade by AMD3100 inhibits experimental abdominal aortic aneurysm expansion through anti-inflammatory effects.* Arterioscler Thromb Vasc Biol, 2014. **34**(8): p. 1747-55.
41. De Clercq, E., et al., *Potent and selective inhibition of human immunodeficiency virus (HIV)-1 and HIV-2 replication by a class of bicyclams interacting with a viral uncoating event.* Proc Natl Acad Sci U S A, 1992. **89**(12): p. 5286-90.
42. Hatse, S., et al., *Chemokine receptor inhibition by AMD3100 is strictly confined to CXCR4.* FEBS Lett, 2002. **527**(1-3): p. 255-62.
43. Cao, G., et al., *Single-cell RNA sequencing reveals the vascular smooth muscle cell phenotypic landscape in aortic aneurysm.* Cell Commun Signal, 2023. **21**(1): p. 113.
44. Pan, J.Y., et al., *miR-206/133b Cluster: A Weapon against Lung Cancer?* Mol Ther Nucleic Acids, 2017. **8**: p. 442-449.
45. Liu, N., et al., *MicroRNA-206 promotes the recruitment of CD8(+) T cells by driving M1 polarisation of Kupffer cells.* Gut, 2022. **71**(8): p. 1642-1655.

Table 1

Table 1. Patient Characteristics

Characteristics	AAA	Healthy ctrl
	n=19	n=19
Age y	68.8±10.1	68.8±9.6
Male	4(21.1%)	4(21.1%)
Coronary heart disease	0(0.0%)	0(0.0%)
Hyperlipidemia	0(0.0%)	0(0.0%)
Diabetes mellitus	1(5.3%)	1(5.3%)
Hypertension	8(42.1%)	2(10.5%)
Smoking	9(47.4%)	4(21.1%)
Maximum abdominal aortic diameter (cm)	5.28±1.0	NA

Data are expressed as a number (percent) or as the mean ± standard deviation. AAA: patients diagnosed with abdominal aortic aneurysm, serum is used. Healthy ctrl: age-matched healthy people committed to physical examination, serum is used.

Figures

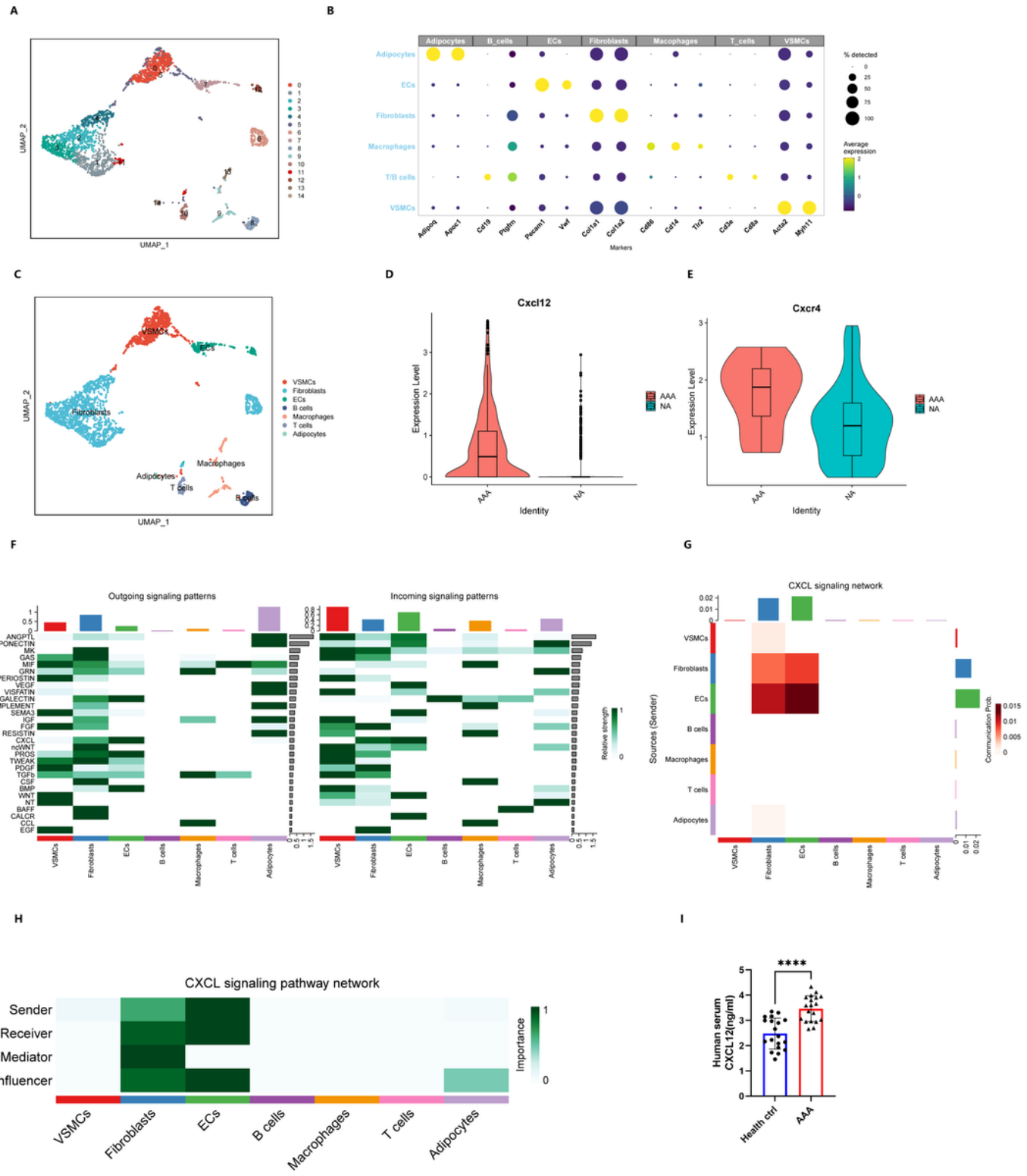

Figure 1

Identified CXCR4/CXCL12 expression in Vascular Smooth Muscle Cells of Aortic Aneurysms

A. The UMAP projection cluster scatter diagram was noted with clusters. **B**. The expression level and expression percentage of marker genes are illustrated on the dot plot. **C**. The UMAP projection cluster scatter diagram was noted with cell types. **D**. Expression level of Cxcl12 in healthy controls and patients

with AAA. **E**. Expression level of Cxcr4 in healthy controls and mice with AAA. **F**. outing and incoming signaling pathway mediated intercellular communication intensity was shown in the heatmap. **G**. CXCL signaling pathway mediated intercellular communication intensity was shown in hierarchy plot heatmap. **H**. Network center score showed the role each cell type played in CXCL signaling pathway network, including sender, receiver, mediator, and influencer. **I**. Serum CXCL12 contents measured in patients with AAA(n=19) and matched healthy individuals (n=19; P<0.0001).

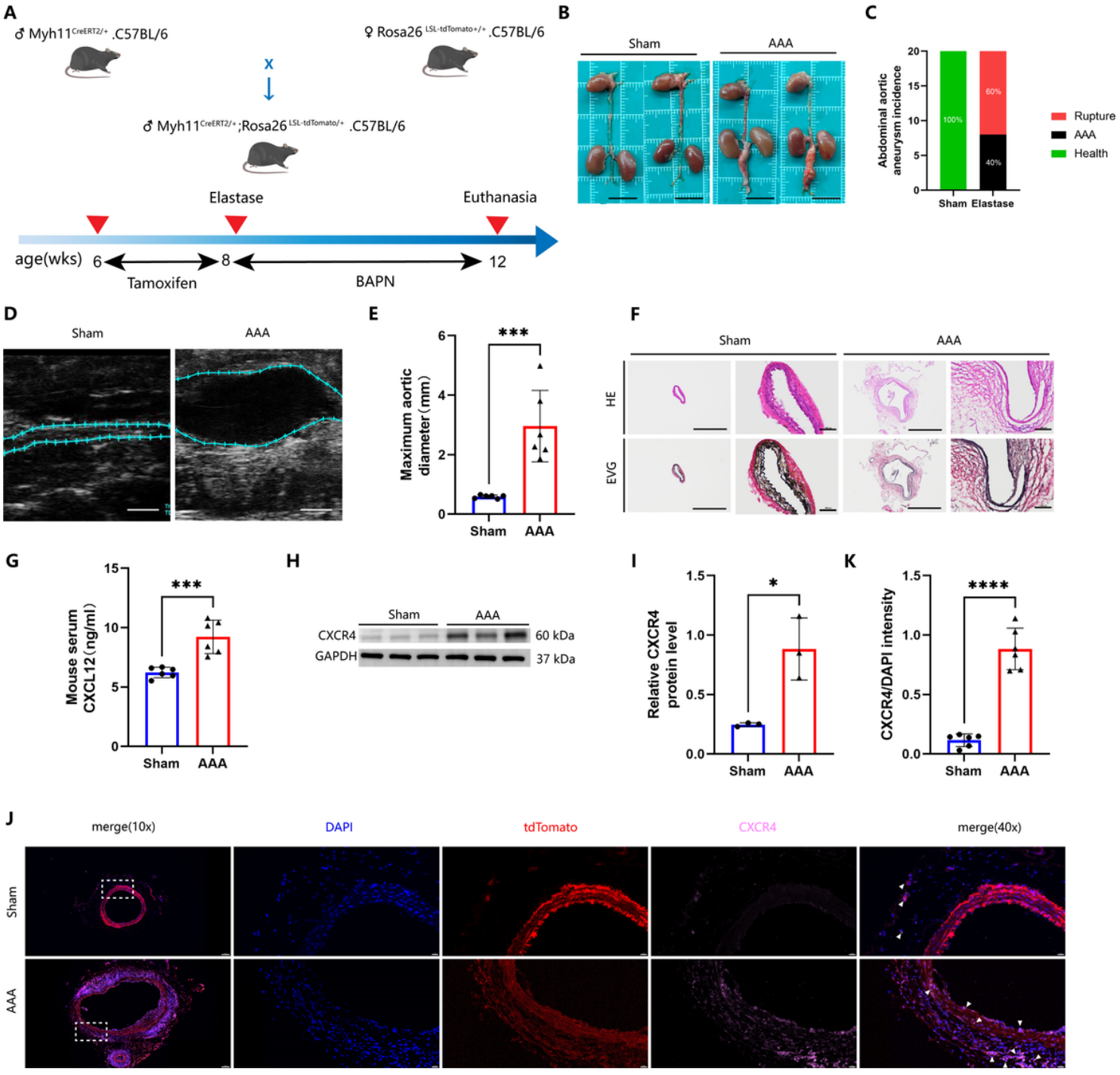

Figure 2

Elastase-induced increase of CXCL12/CXCR4 axis levels in AAA mice

A.Experimental design of AAA mouse model induced by elastase and BAPN. **B**. Representative aorta photographs of sham and AAA mice (scale bar, 1 cm). **C**.Abdominal aortic rupture rate in Sham and AAA groups. **D-E**.Transabdominal ultrasound image of the abdominal aorta and measurements of the maximum diameter of the abdominal aorta (scale bar, 1mm). **E**.Maximum abdominal aortic diameter measurement(n=6; P<0.001). **F**.Representative macroscopic images of hematoxylin and eosin (HE) and Elastic-Van Giessen (EVG) stained sections of the abdominal aorta(scale bars, left: 1000μm, right: 100μm). **G**.Serum CXCL12 levels were detected by ELISA (n=6 per group; P<0.001). **H** and **I**.Western blot analysis of CXCR4 levels in the abdominal aorta of the healthy control and AAA mice (n=3 per group; P<0.05). **J** and **K**, On the basis of SMC lineage tracer tdTomato (red), immunofluorescence staining of CXCR4 (pink) and DAPI (blue) was performed and the level of CXCR4 in aorta is represented by the ratio of CXCR4 to DAPI (n=6; P<0.0001; scale bars, left: 100μm, right: 20μm).

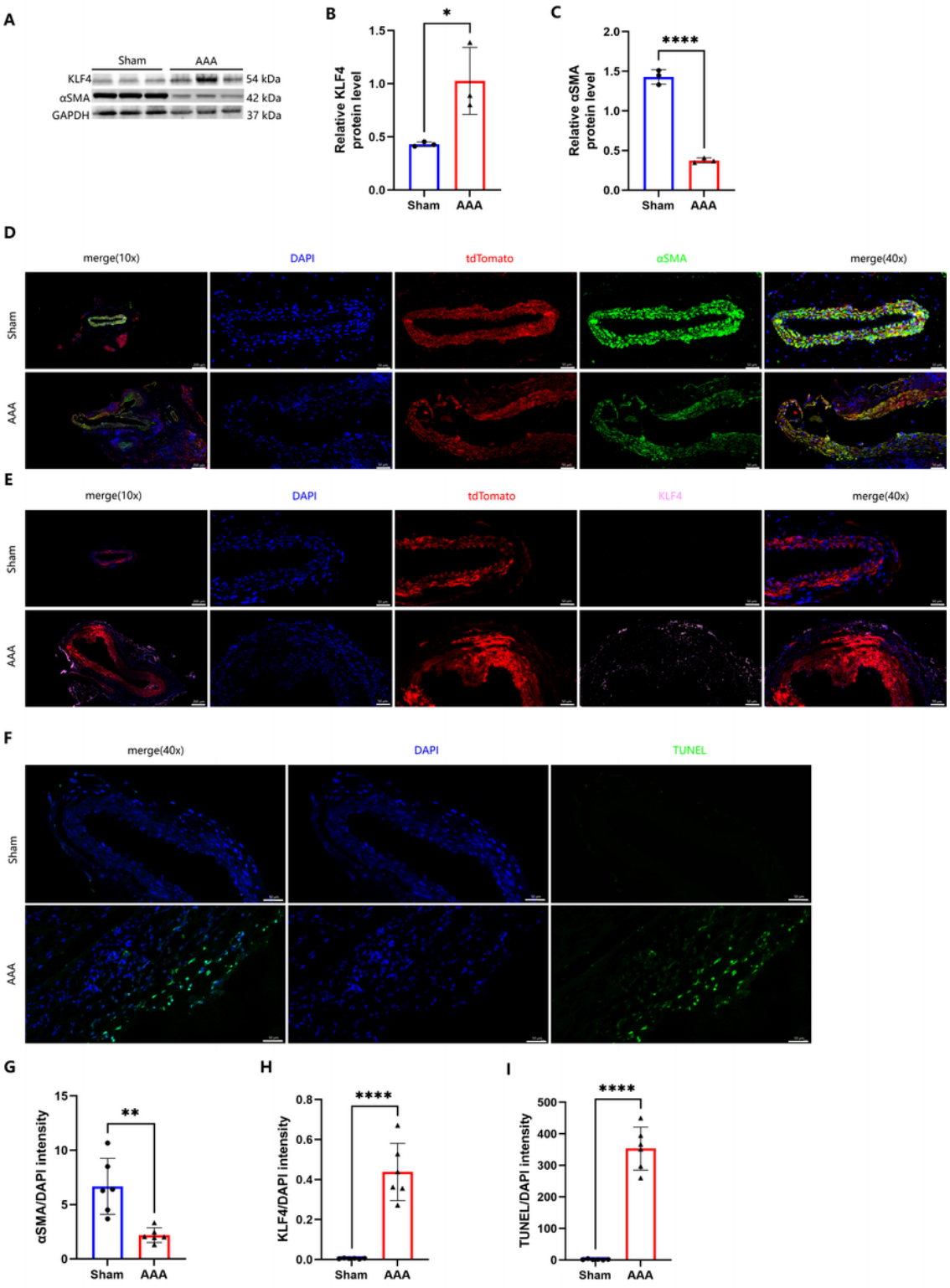

Figure 3

Enhancement of the CXCL12/CXCR4 axis is accompanied by increased phenotypic transformation and apoptosis of smooth muscle cells

A through **C.** Representative Western blot images were used to quantitatively determine αSMA and KLF4 in mouse aortic tissue (n=3 , nonparametric Mann-Whitney U test, **B**,P<0.05; **C**,P<0.0001). **D** and **G**. On the

basis of SMC lineage tracer tdTomato (red), immunofluorescence staining of αSMA (green) and DAPI (blue) was performed and the level of αSMA in aorta is represented by the ratio of αSMA to DAPI (n=6; P<0.01; left: 100μm, right: 20μm). **E** and **H**. On the basis of SMC lineage tracer tdTomato (red), immunofluorescence staining of KLF4 (pink) and DAPI (blue) was performed and the level of KLF4 in aorta is represented by the ratio of KLF4 to DAPI (n=6; P<0.0001; left: 100μm, right: 20μm). **F** and **I**. TUNEL (green) staining and quantitative determination in aorta. Nuclear antistaining with DAPI (blue; n=6, P<0.0001; Scale, 50 μm)

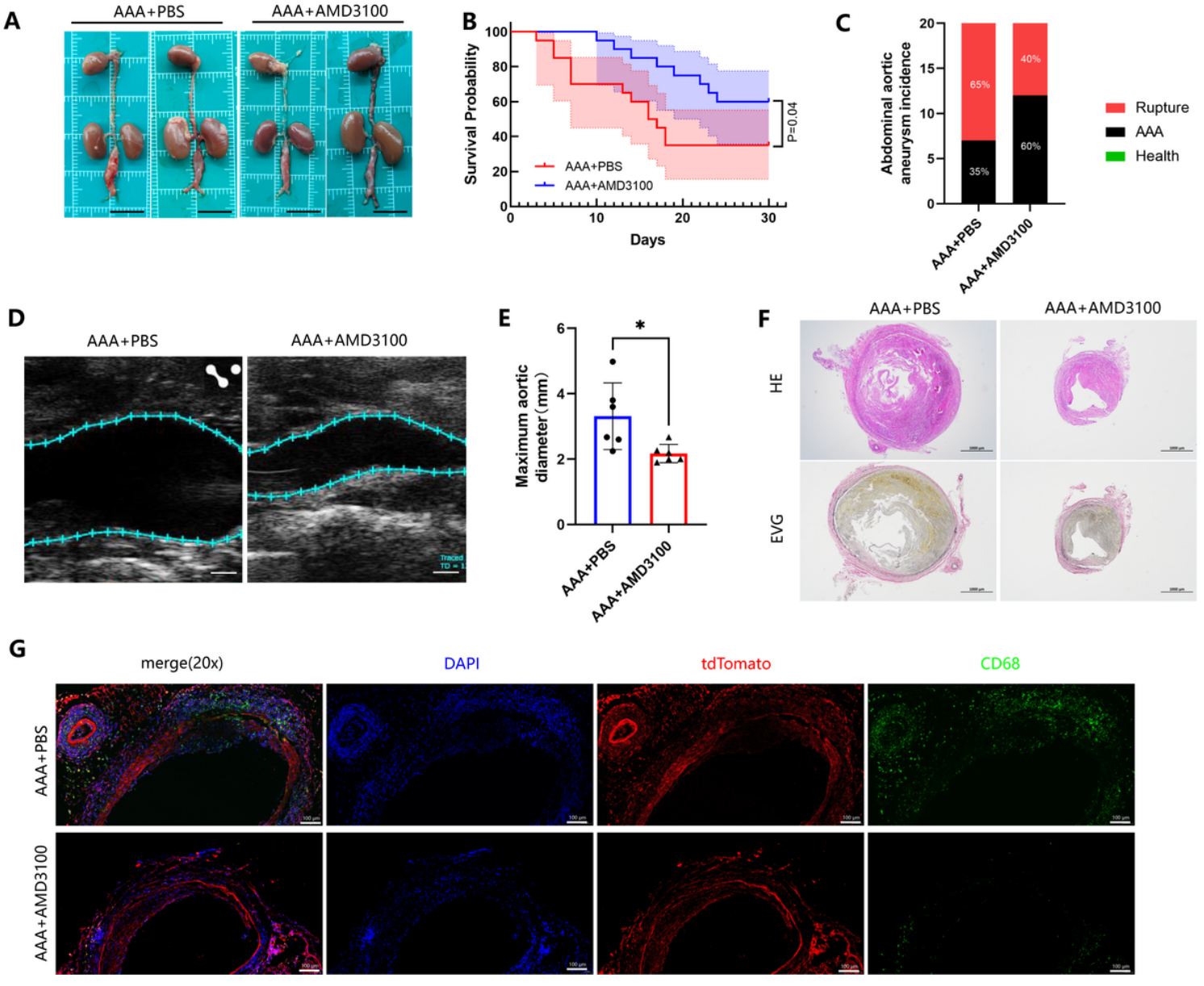

Figure 4

Inhibition of abdominal aortic aneurysm progression in mice by AMD 3100

A. Representative aorta photographs of AAA mice intraperitoneally injected with PBS or AMD33100 (scale bar, 1 cm). **B**.Survival probability was estimated by Kaplan-Meier method and compared by log-rank test (P=0.04; n=20). **C**. Incidence and rupture rate of abdominal aortic aneurysm. **D-E**. Transabdominal

ultrasound image of the abdominal aorta and measurements of the maximum diameter of the abdominal aorta. **F**. Representative images of hematoxylin and eosin (HE) and elastic–Van Gieson (EVG) of AAA mice intraperitoneally injected with PBS or AMD33100;(scale bars, 1000μm). **G**.Representative images of mouse aorta stained with SMC lineage tracer tdTomato (red) and CD68 (green; scale bar, 100μm).

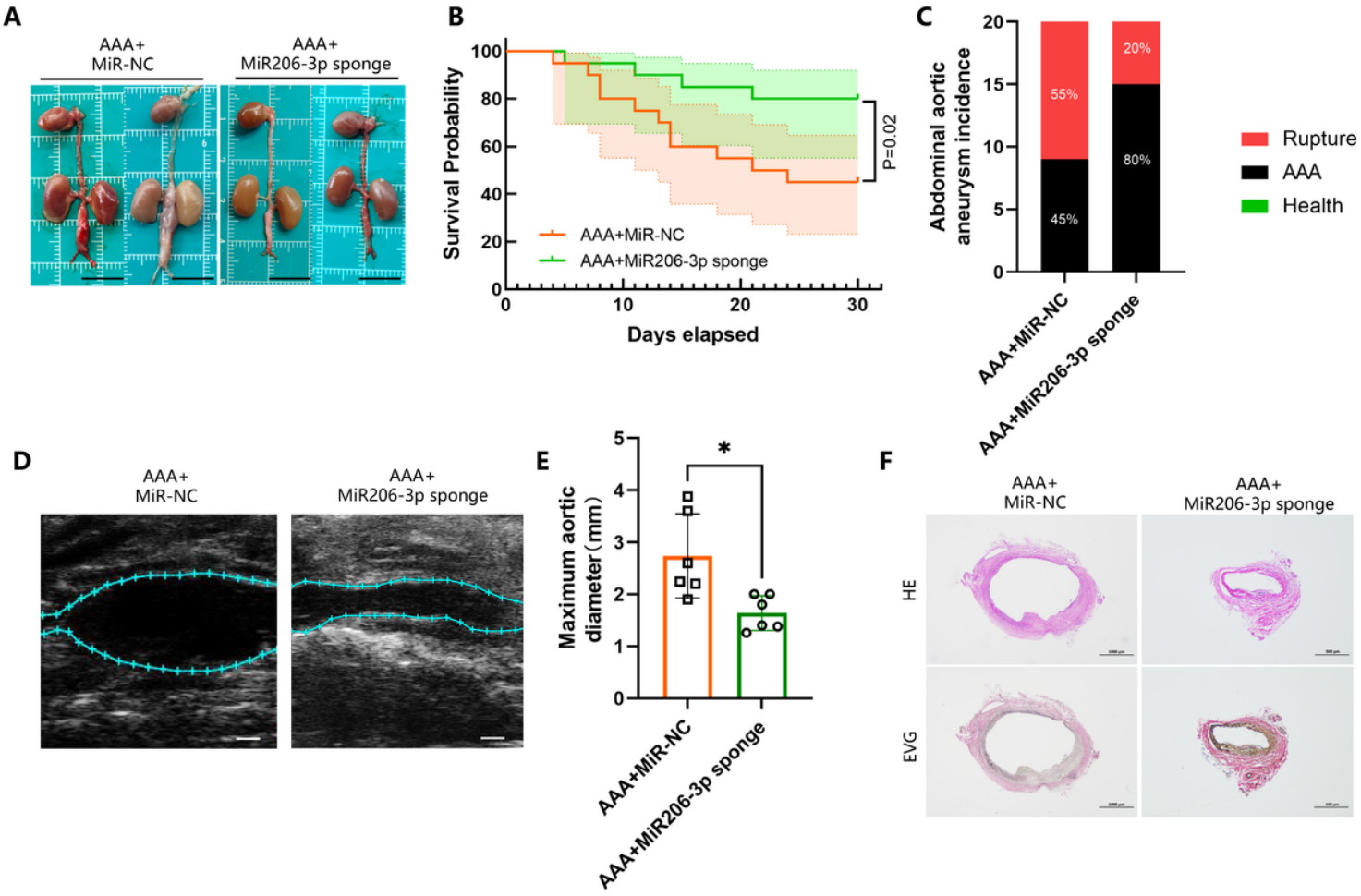

Figure 5

Inhibition of abdominal aortic aneurysm progression in mice by miR206-3p-sponge transfection

A. Representative aorta photographs of AAA mice transfected with AAV2/9-miR-NC or AAV2/9-miR206-3p sponge(scale bar, 1 cm). **B**.Survival probability was estimated by Kaplan-Meier method and compared by log-rank test (P=0.04; n=20 per group). **C**. Incidence and rupture rate of abdominal aortic aneurysm. **D-E**. Transabdominal ultrasound image of the abdominal aorta(scale bar, 1 mm) and measurements of the maximum diameter of the abdominal aorta.(n=6; P<0.05). **F**. Representative images of hematoxylin and eosin (HE) and elastic–Van Gieson (EVG) of AAA mice transfected with AAV2/9-miR-NC or AAV2/9-miR206-3p sponge(scale bars, 1000μm).

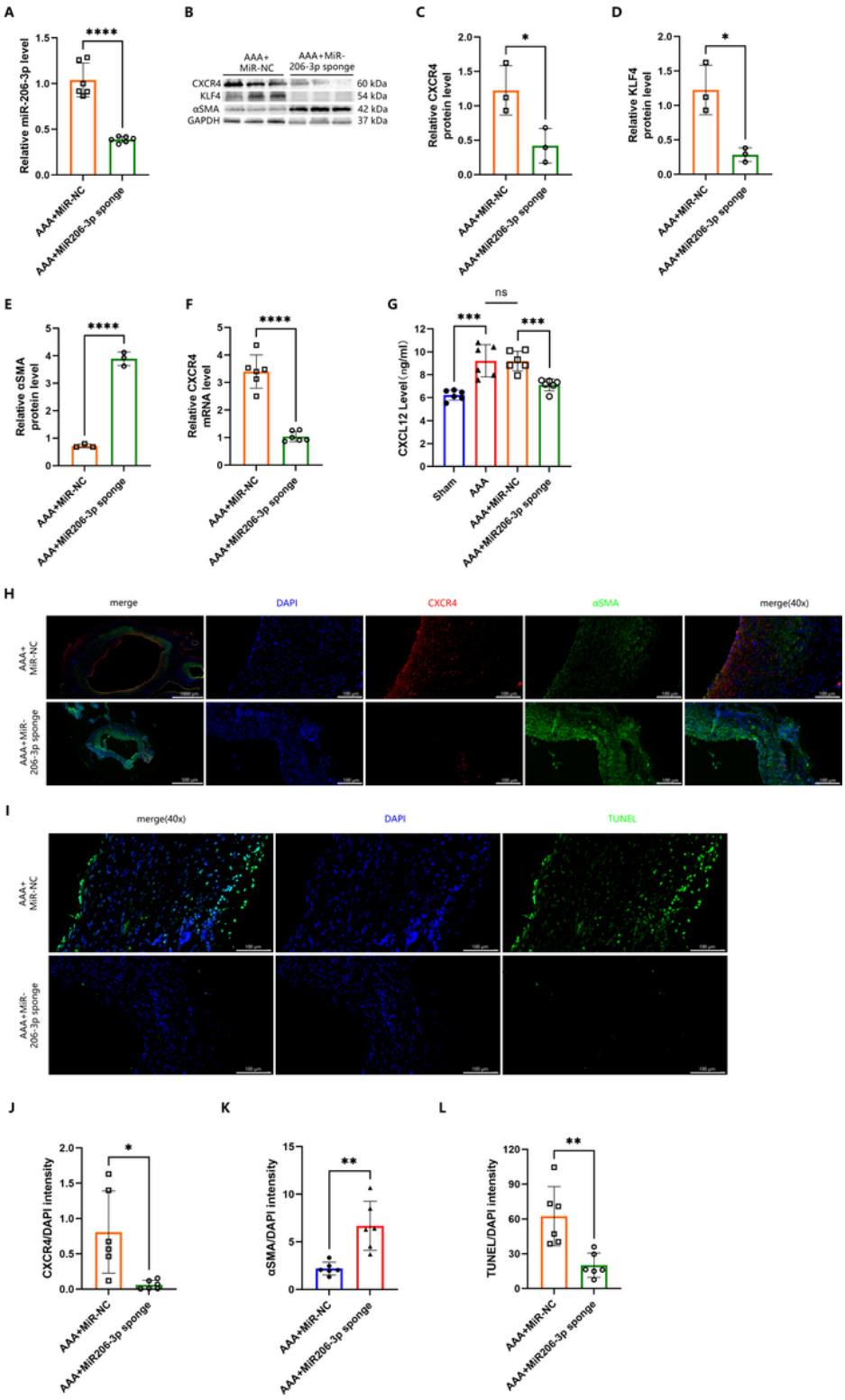

Figure 6

Reduction of CXCR4 expression in abdominal aortic aneurysms and phenotypic transformation and apoptosis in VSMCs by miR206-3p sponge

A. Relative miR206-3p levels in abdominal aorta (n=6, P<0.0001). **B**through **E**. Representative Western blot images were used to quantitatively determine CXCR4 αSMA and KLF4 in mouse aortic tissue (n=3 ,

nonparametric Mann-Whitney U test, B,P<0.05; C,P<0.0001). **F**.Relative CXCR4 mRNA levels in aortic tissues (n=6, P<0.0001). **G**.Serum CXCL12 levels were detected by ELISA (n=6 per group). **H** , **J** and **K**. Immunofluorescence staining of CXCR4 (red), αSMA(green) and DAPI (blue) was performed and the level of CXCR4 and αSMA in aorta is represented by the ratio of CXCR4 and αSMA to DAPI (n=6; **J**,P<0.05; **K**,P<0.05; left: 1000μm, right: 100μm). **I** and **L**. TUNEL (green) staining and quantitative determination in aorta. Nuclear antistaining with DAPI (blue; n=6, P<0.01; Scale, 100 μm)

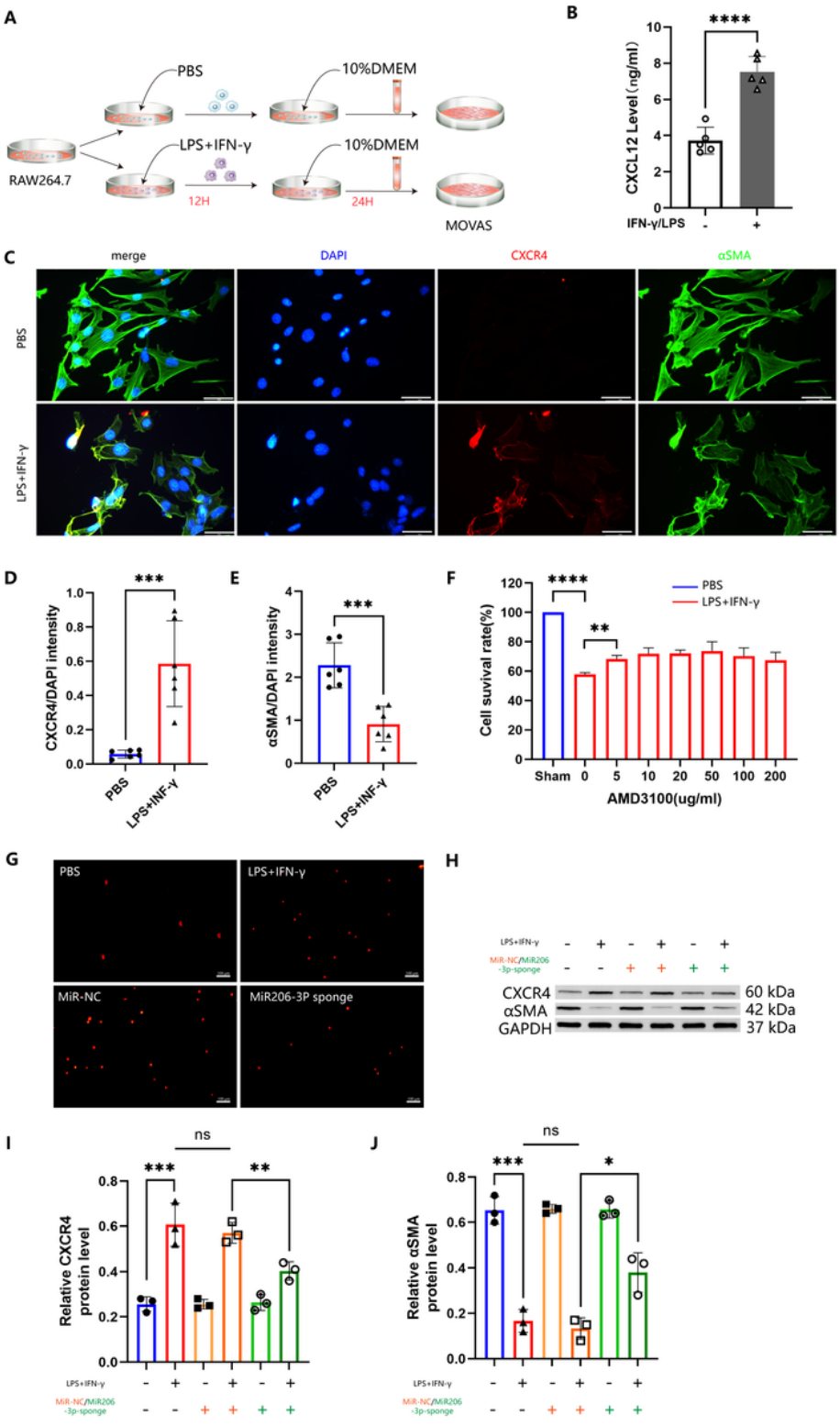

Figure 7

Reduction of phenotypic transformation and apoptosis in MOVAS by miR206-3p-sponge

A. Illustration of the coculture system. LPS/IFN-γ was used to induce RAW264.7differentiation. The culture medium of macrophages was then used to co-culture with MOVAS. **B**. Quantification of CXCL12 content in RAW264.7 culture supernatant with or without LPS/IFN-γ treatment(n=6, P<0.0001). **C-E**. Representative confocal images of CXCR4 (red) and αSMA (green) and filaments in VSMCs treated with or without co-culture (scale bars, 50 μm). **F**. Cell viability of MOVAS after co-culture was detected by CCK-8 assay. **G**. The apoptosis of MOVAS was observed under confocal microscope (red). **H-J**. Representative Western blot images were used to quantitatively determine CXCR4 and αSMA in MOVAS (n=3 , *,P<0.05; **,P<0.01; ***,P<0.001).